



In-situ observation for RH-dependent mixing states of submicron particles containing organic surfactants and inorganic salts

Chun Xiong^{1#}, Binyu Kuang^{1#}, Fei Zhang¹, Xiangyu Pei¹, Zhengning Xu¹, Zhibin Wang^{1,2,3*}

¹College of Environmental and Resource Sciences, Zhejiang University, Zhejiang Provincial Key Laboratory of Organic Pollution Process and Control, Hangzhou, 310058, China

²ZJU-Hangzhou Global Scientific and Technological Innovation Center, Zhejiang University, Hangzhou 311215, China

³Key Laboratory of Environment Remediation and Ecological Health, Ministry of Education, Zhejiang University, Hangzhou, 310058, China

*Correspondence to Zhibin Wang (wangzhibin@zju.edu.cn)

Chun Xiong and Binyu Kuang contribute equally to this work.

Abstract: Aerosol mixing state plays an important role in heterogeneous reactions and CCN activity. Organic surfactants could affect aerosol mixing state through bulk-surface partitioning. However, the mixing state of surfactant containing particles remains unclear due to the lack of direct measurements. Here, in-situ characterizations of mixing state for 20 kinds of submicron particles containing inorganic salts (NaCl and (NH₄)₂SO₄) and atmospheric organic surfactants (organosulfates, organosulfonates, and dicarboxylic acids) were conducted upon relative humidity (RH) cycling by Environmental Scanning Electron Microscopy (ESEM). As RH increased, surfactant shells inhibited water diffusion exposing to inorganic core, leading to notably increased inorganic deliquescence RH (88.3–99.5%) compared with pure inorganic aerosol. Meanwhile, we directly observed obvious Ostwald ripening process, that is, the growth of larger crystals at the expense of smaller ones, in 6 among 10 NaCl-surfactants systems. As a result of water inhibition by surfactant shell, Ostwald ripening in all systems occurred at RH above 90%, which were higher than reported RH range for pure NaCl measured at 27°C (75–77%). As RH decreased, 8 systems underwent liquid-liquid phase separation (LLPS) before efflorescence, showing a strong dependence on organic molecular oxygen-to-carbon ratio (O:C). Quantitatively, LLPS was always observed when O:C ≤ 0.4 and was never observed when O:C > ~0.57. Separation RH (SRH) of inorganic salt-organic surfactant mixtures generally followed the trend of (NH₄)₂SO₄ < NaCl, which is consistent with their salting out efficiencies reported in previous studies. Phase separations were observed after efflorescence for systems without LLPS. Our results provide a unique insight into the consecutive mixing processes of the inorganic-surfactant particles, which would help improve our fundamental knowledge of model development on radiative effect.



29 1 Introduction

30 Atmospheric particles are complex mixtures of multiple inorganic and organic matters (Pöschl, 2005). When relative
31 humidity (RH) varies, particles can undergo phase transitions such as deliquescence (Peng et al., 2001), efflorescence
32 (Takahama et al., 2007), and liquid–liquid phase separation (LLPS) (Martin, 2000), hence altering mixing state. The transition
33 of aerosol mixing state can influence gas uptake, hygroscopicity, cloud condensation nuclei (CCN) activity, and radiative
34 absorption (Riemer et al., 2019).

35 Upon hydration, previous studies suggested that different mixing state between inorganic and organic matters influence
36 aerosol hygroscopic behaviours (e.g., deliquescence) and solar radiation (Peng et al., 2016; Li et al., 2021). For instance, Peng
37 et al. (2016) observed deliquescence RH of internal mixed NaCl–oxalic acid at 73%, being slightly lower than that of pure
38 NaCl (75%) because of the interactions between inorganic and organic matters. However, Li et al. (2021) found a different
39 deliquescence process if ammonium sulfate (AS) was coated by secondary organic aerosol, the organic shell firstly dissolved
40 at ~50% RH but water uptake of the AS core was inhibited, leading to a higher deliquescence RH of AS (~83–90%). By
41 cryogenic transmission electron microscopy (cryo–TEM), Zhang et al. (2022) directly observed collected particles from a rural
42 site remained LLPS (inner inorganic phase and outer organic phase) between organic matter and inorganic salts when RH
43 raised to $75 \pm 2\%$ and $86 \pm 2\%$, but LLPS disappeared when RH increased to $95 \pm 2\%$. They later suggested that LLPS with
44 higher ratio of organic coating thickness to black carbon size can drive black carbon from inorganic core to organic particle
45 coatings, which could result in 18% radiative absorption overestimation of black carbon aerosols in climate models by
46 assuming a core-shell particle structure.

47 Upon dehydration, phase separation has been frequently observed in ambient particles (You et al., 2012; Ting et al., 2018;
48 Zhang et al., 2020; Zhang et al., 2022). For example, LLPS occurred at $> 90\%$ RH for particles containing water extraction of
49 collected atmospheric particles in Atlanta and simulations indicated that LLPS can decrease particle uptake of N_2O_5 thus
50 increase concentrations of gas–phase NO_3 and N_2O_5 (You et al., 2012). Factors contributing to LLPS, e.g. oxidation levels
51 (Bertram et al., 2011; Song et al., 2017; Song et al., 2019), organic fraction (Ciobanu et al., 2009; Song et al., 2012b), inorganic
52 species (You et al., 2013), and temperature (You and Bertram, 2015; Roy et al., 2020) have been discussed for some specific
53 inorganic–organic or organic–organic systems in literature. Song et al. (2012a) and You et al. (2013) found LLPS always
54 occurred for $\text{O}:\text{C} < \sim 0.5$, never occurred for $\text{O}:\text{C} > 0.8$, and when $\text{O}:\text{C}$ was between 0.5 and 0.8, LLPS was depended on
55 inorganic species. Organic fraction showed controversial effects on LLPS (Bertram et al., 2011; Song et al., 2012b) since
56 Bertram et al. (2011) found a weak effect of organic fraction on LLPS for 8 out of 11 AS–organic systems but the rest systems
57 exhibited a quantifiable dependence of separation RH (SRH) on organic fraction. You et al. (2013) reported SRH among out
58 of 20 organics generally followed the trend of $(\text{NH}_4)_2\text{SO}_4 \geq \text{NH}_4\text{HSO}_4 \geq \text{NaCl} \geq \text{NH}_4\text{NO}_3$, which is consistent with
59 their previous reported salting out efficiencies. Temperature did not strongly affect SRH between 253–290 K for AS–organics
60 (O'brien et al., 2015; You and Bertram, 2015) and NaCl–organics systems (Roy et al., 2020). Recently, dry rate (Altaf and



61 Freedman, 2017; Altaf et al., 2018) and size effect (Freedman, 2020; Ott and Freedman, 2021) on LLPS were found for
62 submicron particles. Undergoing drying by slow rate ($\sim 27\%$ per minute), phase separation of AS-pimelic acid system occurred
63 in larger particles (75 \sim 322 nm diameter), but smaller particles (below 25 \sim 135 nm diameter) were homogeneous. In slow
64 drying rates (0.04 to 0.08% RH per second), particles with diameter below 43 nm were homogeneous but larger particles (28
65 \sim 629 nm) were mainly phase-separated (Altaf and Freedman, 2017). Freedman (2020) further explained that LLPS is scarcely
66 occurred in smaller particles as smaller particles cannot overcome the energy barrier needed to form a new phase.

67 Dicarboxylic acids (Ruehl and Wilson, 2014), organosulfates (Bruggemann et al., 2020; Reed et al., 2022), and
68 organosulfonates (Bruggemann et al., 2020; Guo et al., 2020) are important organic constituents in secondary organic aerosol.
69 Primary emission and secondary transition were major sources of dicarboxylic acids and their mass contribution of
70 dicarboxylic acids to total particulate carbon exceeds 10% (Römpp et al., 2006; Ho et al., 2010; Hyder et al., 2012).
71 Organosulfates and organosulfonates, as significant reservoirs of sulfur, comprise an estimated 5%–30% of the total organic
72 aerosol mass (Tolocka and Turpin, 2012; Reed et al., 2022). Above mentioned organics contain both hydrophilic (e.g., sulpho
73 group) and hydrophobic groups (e.g., alkyl group), showing surface activity and causing bulk–surface partitioning (Noziere,
74 2016; Ruehl et al., 2016), hence affecting individual aerosol morphology (Kwamena et al., 2010). However, mixing state of
75 submicron inorganic–surfactant particles remain unclear due to the lack of direct measurements. Here, we directly observed
76 mixing states of submicron particles containing inorganic salt and organic surfactant with varying organic volume fraction
77 (OVF) upon humidity cycling by Environmental Scanning Electron Microscopy (ESEM). Our results could provide unique
78 insights into the dynamic evolution of inorganic–surfactant particles under fluctuating atmospheric conditions.

79 **2 Materials and Methods**

80 **2.1 Chemicals**

81 NaCl and AS were purchased from Sinopharm chemical reagent (purity $\geq 99.8\%$) and Sigma Aldrich (purity $\geq 99\%$),
82 respectively. The studied organic substances include 10 surface active organics (five organosulfonates, three organosulfates
83 and two dicarboxylic acids). The five organic sulfonates were sodium propane sulfonate ($C_3H_7SO_3Na$), sodium butane
84 sulfonate ($C_4H_9SO_3Na$), sodium pentane sulfonate ($C_5H_{11}SO_3Na$), sodium heptane sulfonate ($C_7H_{15}SO_3Na$), sodium octane
85 sulfonate ($C_8H_{17}SO_3Na$). The three organic sulfates were sodium methyl sulfate (CH_3SO_4Na), sodium ethyl sulfate
86 ($C_2H_5SO_4Na$) and sodium octyl sulfate ($C_8H_{17}SO_4Na$). Two dicarboxylic acids were pimelic acid (PA) and phenylmalonic acid
87 (PhMA). Relevant properties of used chemicals were summarized in **Table 1**. These organic surfactants were of various
88 solubilities, from sparingly soluble (e.g., 0.07 mol L^{-1} for $C_8H_{17}SO_4Na$) to highly soluble (e.g., 2.7 mol L^{-1} for $C_4H_9SO_3Na$).
89 O:C ratios were from 0.38 to 4, covering most of the molar ratios in the atmosphere (0.1–1.0) (You et al., 2013). The studied
90 organic substances contain functional groups such as sulfonates, sulfates, carboxylic acids and aromatics, which were
91 universally detected in atmospheric aerosol samples (Takahama et al., 2007).



92

93

Table 1 Organic surfactants and their relevant properties investigated in this study.

Species	Compounds	Formula	*Solubility (mol L ⁻¹)	O:C	Purity	Supplier
Organic sulfonate	Sodium propane sulfonate	C ₃ H ₇ SO ₃ Na	2.0	1.00	>98%	Aladdin
	Sodium butane sulfonate	C ₄ H ₉ SO ₃ Na	2.7	0.75	≥99%	Aladdin
	Sodium pentane sulfonate	C ₅ H ₁₁ SO ₃ Na	2.3	0.60	98%	Aladdin
	Sodium heptane sulfonate	C ₇ H ₁₅ SO ₃ Na	1.9	0.43	98%	Macklin
	Sodium octane sulfonate	C ₈ H ₁₇ SO ₃ Na	0.9	0.38	≥99%	Macklin
Organic sulfate	Sodium methyl sulfate	CH ₃ SO ₄ Na	2.1	4.00	98%	Energy Chemical
	Sodium ethyl sulfate	C ₂ H ₅ SO ₄ Na	0.4	2.00	98%	Meryer
	Sodium octyl sulfate	C ₈ H ₁₇ SO ₄ Na	0.07	0.50	99%	Rhawn
Dicarboxylic acid	Pimelic acid (PA)	C ₇ H ₁₂ O ₄	0.31	0.57	99%	Macklin
	Phenylmalonic acid (PhMA)	C ₉ H ₈ O ₄	0.7	0.44	98%	Aladdin

94

95 * <https://comptox.epa.gov/> (last access: 12 March, 2023)

96 2.2 Aerosol generation and collection

97 The process of aerosol generation and collection was detailedly described by Xiong et al. (2022). In brief, particles were
 98 nebulized from solutions of organic and inorganic matters (~5 g L⁻¹) mixed with deionized water (Millipore, resistivity = 18.2
 99 MΩ). After drying (RH < 15%) by a silica-gel diffusion dryer, particles were deposited with an eight stage non-viable particle
 100 sizing sampler (Models BGI20800 Series, BGI Incorporation) onto 400 mesh copper grids coated with carbon films
 101 (Zhongjingkeyi Films Technology Co. Ltd.). Copper grids were mounted on the 7th stage, selecting particles with aerodynamic
 102 size of 0.7–1 μm. Collected samples were stored under dry condition (RH < 10%) and were immediately characterized within
 103 24 hours to avoid possible sample aging.



104 2.3 Mixing state observation

105 Mixing state was observed by Environmental Scanning Electron Microscopy (ESEM, Thermo Quattro S) with a
106 temperature-controlled stage. The RH in chamber was controlled by adjusting the temperature (± 0.1 °C) at a predefined
107 pressure (610 Pa). Temperature varied between 0.1 to ~ 25 °C, which has negligible influence on the LLPS of AS-organic
108 (O'Brien et al., 2015; You and Bertram, 2015) and NaCl-organic systems (Roy et al., 2020). In each experiment, the RH raised
109 from low ($\sim 30\%$) to high condition ($\sim 100\%$) at the change rate of $2\text{--}3\%$ RH min^{-1} . High RH lasted for at least 5 minutes for
110 equilibrium, promising complete dissolution (O'Brien et al., 2015). Then, RH decreased to dry condition at similar change rate.
111 Cloud parcel modelling suggests that atmospheric RH fluctuations typically occur from 0 to 3.6% min^{-1} (Pöhlker et al., 2014).
112 Therefore, we assume that the water uptake in our experiments approximates atmospheric conditions (Shiraiwa et al., 2013).
113 Images of mixing states during the whole RH period were acquired at an electron acceleration voltage of 30 kV. The images
114 were recorded with line scanning rates of $3\text{--}5$ μs to minimize the possible beam damage (O'Brien et al., 2015). Each image
115 contained at least 5 particles.

116 3 Results and Discussion

117 3.1 Mixing states upon hydration

118 Deliquescence RH (DRH) and Efflorescence RH (ERH) of pure NaCl (**Fig. 1a–d** and **Fig. S1a–b**) and AS particles (**Fig.**
119 **2a–d** and **Fig. S1c–d**) were firstly tested via the experimental setup. DRH of NaCl and AS were observed at $80.9 \pm 0.1\%$
120 (literature: $77 \pm 1\%$ (Pöhlker et al., 2014)) and $82.1 \pm 0.6\%$ (literature: 82.0% (Onasch et al., 1999)). ERH of NaCl and AS
121 were $48.3 \pm 0.4\%$ (literature: $48 \pm 2\%$ (Zeng et al., 2014)) and $30.7 \pm 0.9\%$ (literature: $31 \pm 1\%$ (Cheng and Kuwata, 2023)).
122 Generally, the experimental DRH and ERH values correspond well with those in literature, confirming the reliability of the
123 experimental setup. DRH of NaCl showed slight deviation by about nearly 4%, which could be explained by kinetic effects
124 when the system had not reached full equilibrium (Pöhlker et al., 2014). Before deliquescence, the substrate-supported NaCl
125 and AS particles both showed substantial water uptake, forming an aqueous halo around a solid core. Similar observational
126 results of NaCl and AS have been reported, and could be explained by interactions at the sample/substrate interface, which
127 plays an important role in such gradual phase transition as additional energy term (Wise et al., 2008; Pöhlker et al., 2014).

128 **Figure 1e** and **Fig. 2e** illustrate the two separated phases with dark core (blue arrow) and bright shell (green arrow) of
129 dry deposited NaCl- $\text{C}_2\text{H}_5\text{SO}_4\text{Na}$ and AS- $\text{C}_2\text{H}_5\text{SO}_4\text{Na}$ particles. The dark cores are indicated to be inorganics, because darker
130 regions are characteristic of areas with higher atomic number elements (e.g., Cl) and/or a thicker sample region (Laskin et al.,
131 2006; O'Brien et al., 2015). Phase separations with core-shell structure were observed for all studied inorganic-surfactant
132 systems. This may be attributed to the size range of particles we investigated ($0.7\text{--}1$ μm), since inorganic-surfactants particles
133 with such size range might overcome the energy barrier needed to form a new phase (Altaf and Freedman, 2017; Altaf et al.,
134 2018; Freedman, 2020; Ott and Freedman, 2021).

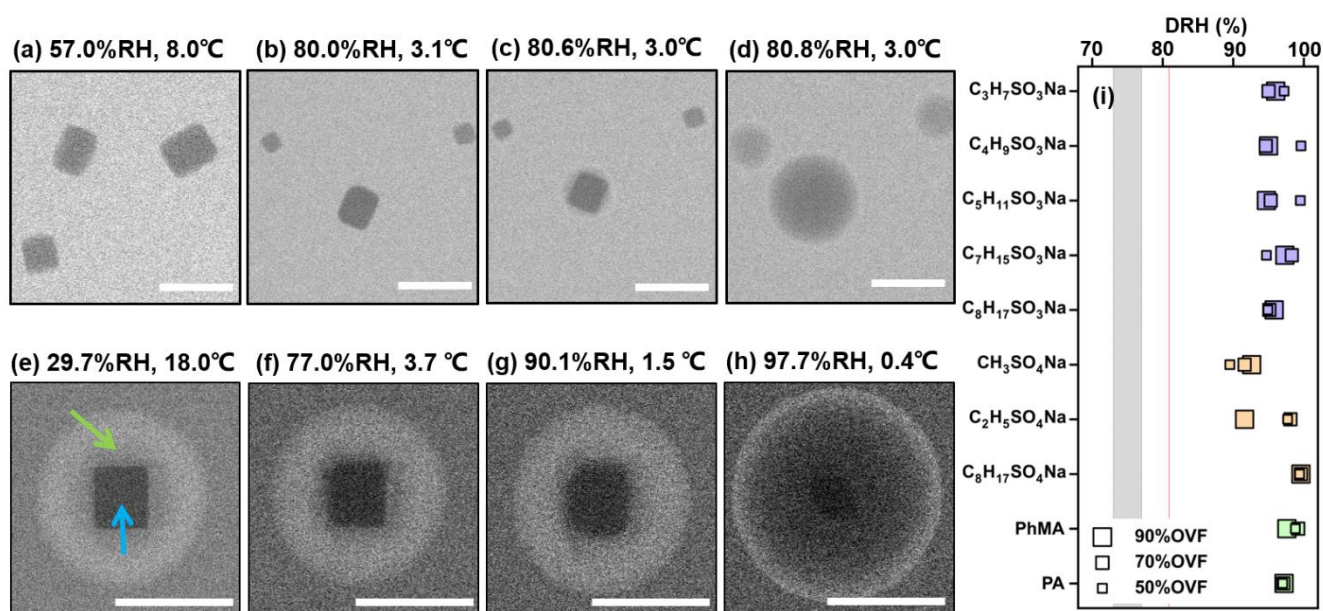


135 When RH increased from dry, as organic phase slowly absorbed water, NaCl and AS cores were not fully dissolved at
136 RH of 90.1% and 91.7% (**Fig. 1g and Fig. 2g**), respectively, being notably higher than their DRH. The phenomenon was found
137 for all NaCl–surfactant and AS–surfactant systems and the DRH of the inorganic salts were ranged in 88.3–99.5% (**Fig. 1i**
138 **and Fig. 2i**). Laskina et al. (2015) measured the DRH of pure AS and NaCl at submicrometer (100 nm) and supermicrometer
139 (3–10 μm) size ranges by hygroscopic tandem differential mobility analyzers (HTDMA) and MicroRaman Spectroscopy,
140 respectively, and the deviations between them were both within 3%, indicating that DRH of pure AS and NaCl showed weak
141 size dependence (> 100 nm). In addition, (Cheng and Kuwata, 2023) used low-temperature hygroscopicity tandem differential
142 mobility analyzer (Low-T HTDMA) and observed consistent DRH of NaCl and AS within experimental error under
143 temperature ranged in -10 °C to 22.5 °C, suggesting that the DRH of NaCl and AS experience a neglect temperature
144 dependence. According to the above-mentioned studies, DRH of pure AS and NaCl showed weak size dependence (> 100 nm)
145 and temperature dependence in our experiment, and we therefore concluded that surfactant shell inhibits water diffusion
146 exposing to inorganic cores, resulting in delays of deliquescence of inorganic cores. The inhibition of surfactant shell could be
147 triggered by increased viscosity with raised RH, since reported studies have reported that organic shells can transform from
148 solid to semisolid with high viscosity at wet condition (Zhang et al., 2018). In a RH-constrained lab study at constant room
149 temperature, Li et al. (2021) also observed organic coating of secondary organic aerosol (oxidizing α -pinene) started to
150 deliquesce first, but the phase changes of AS cores from solid to liquid took place at 83–90% RH, lower than those in the
151 current study. This was possibly caused by the water diffusion coefficient through organic phase, which could be affected by
152 organic species and environment parameters such as temperature. Given by Nguyen et al. (2017), the diffusion coefficient of
153 a water molecule through an organic shell could be decreased by lower temperature. In the current study, higher RH in the
154 ESEM chamber was achieved by decreasing temperature, thus might decrease diffusion coefficient of water in organic
155 surfactant and lead to higher DRH than those in Li et al. (2021). Previous study and the current work indicated the phenomenon
156 (water inhabitation by organic coating) to be a common and important procedure in affecting ambient aerosol hygroscopicity,
157 because inorganic–organic core–shell structures were ubiquitous observed in field (Li et al., 2016; Unga et al., 2018; Xu et al.,
158 2020; Li et al., 2021; Wang et al., 2021; Zhang et al., 2022). Though the water inhabitation of organic shell in the current study
159 was observed at temperature much lower than room temperature, it is meaningful and may affect aerosol properties in some
160 special area such as polar regions (Lambert et al., 2013; Kirpes et al., 2022; Zavačka et al., 2022) or winter time period (Xu et
161 al., 2021; Zhang et al., 2021) where are characteristic with low-temperature environment.

162 As previous study believed that deliquescence on hydration for inorganics independent of circumstances, **Fig. 3** illustrates
163 an unexpected phase transition of NaCl cores coated with $\text{C}_2\text{H}_5\text{SO}_4\text{Na}$ (70% OVF). As shown in **Fig. 3a**, a droplet with several
164 NaCl cores was observed at 97.0% RH since discussed above that organic shell inhibits water diffusion. NaCl cores in droplet
165 were a bigger one (marked by white square) and the rest were smaller. When RH gradually raised (**Fig. 3b–c**), as smaller NaCl
166 cores serially deliquesced and dissolved, the size of the bigger NaCl core surprisingly increased, indicating a simultaneous
167 NaCl recrystallization at the expense of smaller ones (i.e., Ostwald ripening) (Boistelle and Astier, 1988). After other small



168 particles totally dissolve, the bigger NaCl core deliquesced and fully dissolved at 99.5% RH (**Fig. 3d**). A previous study
 169 reported “efflorescence upon hydration” for 1:1 mixed NaCl-gluconic acid and AS-gluconic acid by optical tweezer (Zhu et
 170 al., 2022). Based on IR spectrum, they found the coexistence of partial efflorescence mixed state, ultraviscous state and liquid
 171 state during “efflorescence upon hydration” period, indicating an unstable crystal and concentrated liquid state of NaCl. In this
 172 circumstance, Ostwald ripening can take place. Ostwald ripening was triggered by the decrease of total system free energy,
 173 since dissolved small and effloresced big crystals reduce the total system free energy (Voorhees, 1985). We directly and
 174 observed obvious Ostwald ripening processes in 6 among 10 NaCl–surfactants systems. As a results of water inhibition by
 175 surfactant shell discussed above, Ostwald ripening here all occurred at RH above 90%, which were notably higher than reported
 176 75%–77% for pure NaCl measured by X-ray microspectroscopy at 27°C (Pöhlker et al., 2014).

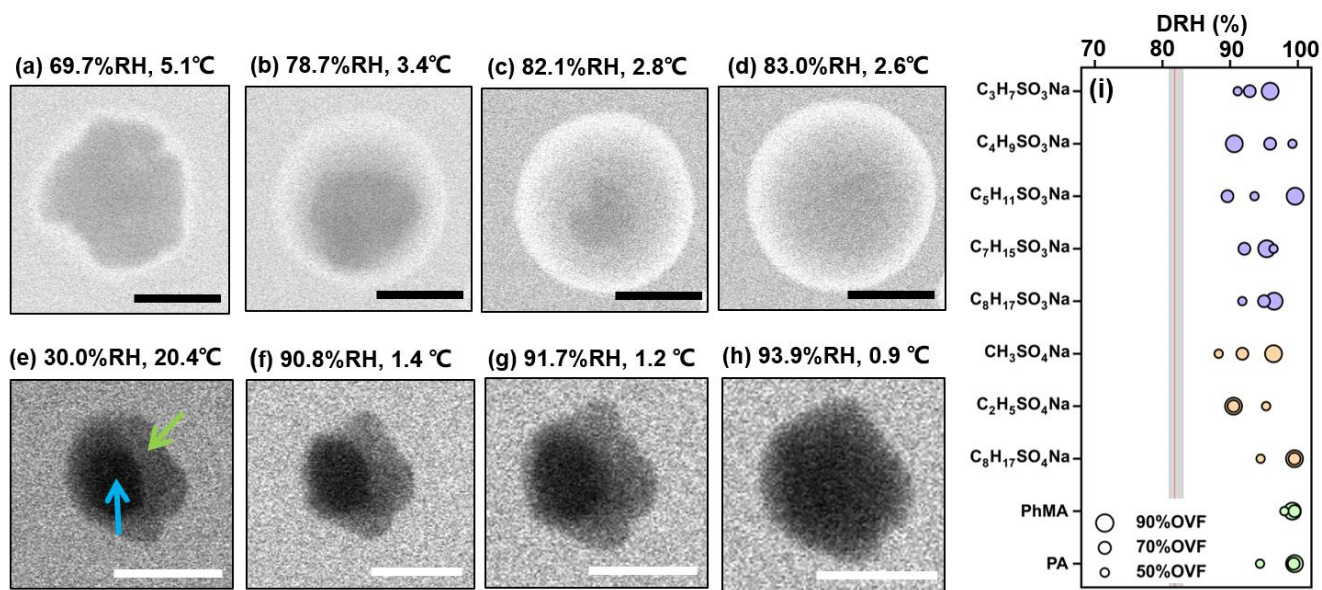


177
 178
 179 **Figure 1.** ESEM images of (a–d) pure NaCl and (e–h) NaCl–C₂H₅SO₄Na (70% OVF) with different RH. Blue and green
 180 arrows indicate the inorganic phase and organic phase, respectively. DRH values of inorganic core for NaCl–surfactants
 181 systems (i). Grey area represents DRH range of NaCl obtained from Peng et al. (2022) Red line indicates the measured DRH
 182 of pure NaCl (80.9 ± 0.1%). Scale bars were 1 μm.

183



184



185

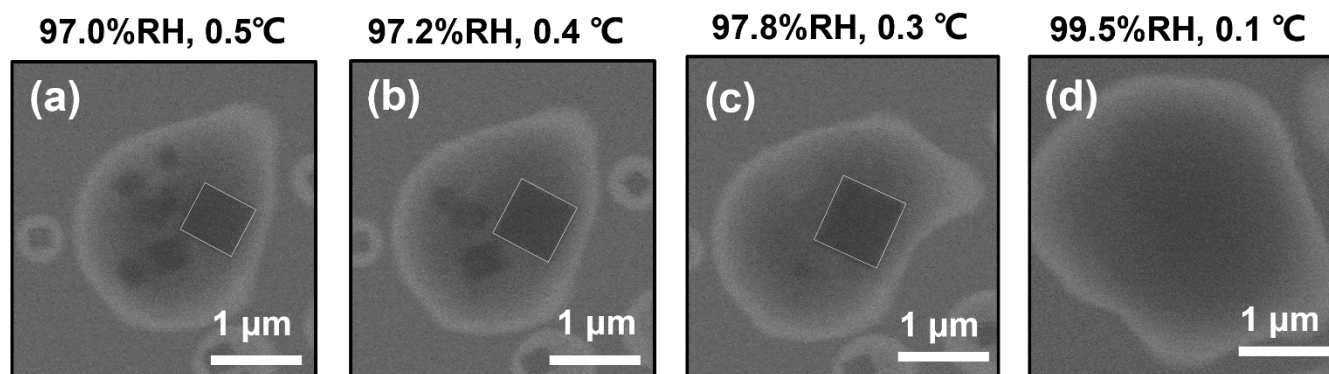
186

187 **Figure 2.** ESEM images of (a–d) pure AS and (e–h) AS–C₂H₅SO₄Na (50% OVF) with different RH. Blue and green arrows
 188 indicate the inorganic phase and organic phase, respectively. (i) DRH values of inorganic core for AS–surfactants systems.
 189 Grey area represents DRH range of AS obtained from Peng et al. (2022) Red line indicates the measured DRH of pure AS
 190 (82.1 ± 0.6%). Scale bars were 1 μm.

191



192



193

194

195

196

Figure 3. ESEM images of Ostwald ripening for NaCl-C₈H₁₇SO₄Na (50% OVF) particle. White square indicates the biggest NaCl core (assumed square) in droplet. The biggest NaCl grew larger (recrystallization) while the small NaCl cores dissolved.



197 3.2 Mixing states upon dehydration

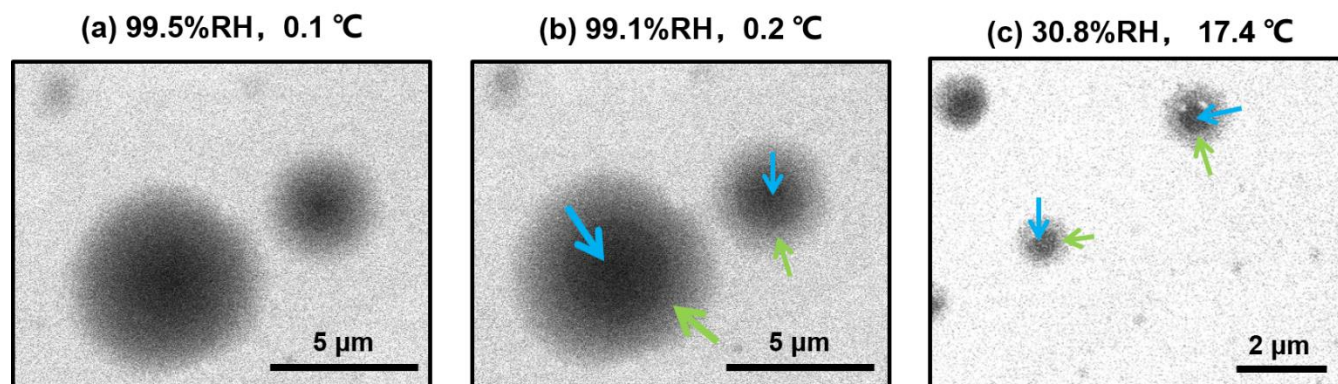
198 LLPS

199 In **Fig. 4a**, AS-C₈H₁₇SO₄Na (50% OVF) was homogeneous under RH of 99.5%. When RH decreased to 98.2%, the
200 particles showed two separated liquid phases (i.e., LLPS) with a dark inner phase and a light outer phase (**Fig. 4b**), which were
201 highlighted by the blue and green arrows. In addition, the AS-C₈H₁₇SO₄Na remained LLPS when RH continue to decline until
202 efflorescence of inner inorganic phase occurred (**Fig. 4c**). In our study, 8 among 20 chemical systems underwent LLPS,
203 including 4 AS-organic systems and 4 NaCl-organic systems. **Fig. 5** illustrates the relationship between LLPS occurrence and
204 molar ratios (O:C and H:C) of the surface-active organics, as well as reported results of other binary inorganic-organic systems
205 in You et al. (2013) and O'brien et al. (2015). Firstly, no trend was observed between LLPS occurrence and H:C of the organics.
206 This was consistent with results in previous studies (Bertram et al., 2011; Song et al., 2012a; You et al., 2013). An apparent
207 trend was found between O:C ratio and LLPS occurrence for different systems, that is, LLPS of inorganic-organic particles
208 were more likely to occurred when O:C ratio was low. Quantitatively, LLPS was always observed for O:C < 0.4 and never
209 observed for O:C ≥ ~0.57 (grey area) was found for NaCl-surfactants and AS-surfactants systems. You et al. (2013) reported
210 that LLPS always occurred for O:C < 0.5 and was never observed for O:C ≥ 0.8 for NaCl-organics and AS-organics with
211 organic-to-inorganic mass ratio of 2 ± 0.1, which was different from our results. This could be attributed to the different
212 chemical systems.

213 In order to analyze the effect of inorganic salts in LLPS, we compared SRH of systems which contained same organic
214 matters but different inorganic salts. Results showed that SRH of AS-C₈H₁₇SO₄Na (70% OVF), AS-C₈H₁₇SO₃Na (90% OVF),
215 AS-PhMA (90% OVF) and AS-PA (90% OVF) were 98.7 ± 0.5%, 81.3 ± 1.2%, 97.9 ± 1.0% and 98.5 ± 0.8%, and were all
216 notably higher than SRH of corresponding NaCl-containing systems (92.5 ± 3.9%, 56.4 ± 1.2%, 85.6 ± 3.6% and 66.7 ± 0.8%),
217 respectively. This was attributed to different salting out efficiency of inorganic salts, since You et al. (2013) found the SRH of
218 inorganic-organic mixtures followed the trend of (NH₄)₂SO₄ ≥ NH₄HSO₄ ≥ NaCl ≥ NH₄NO₃, which were generally consistent
219 with their salting out efficiency.

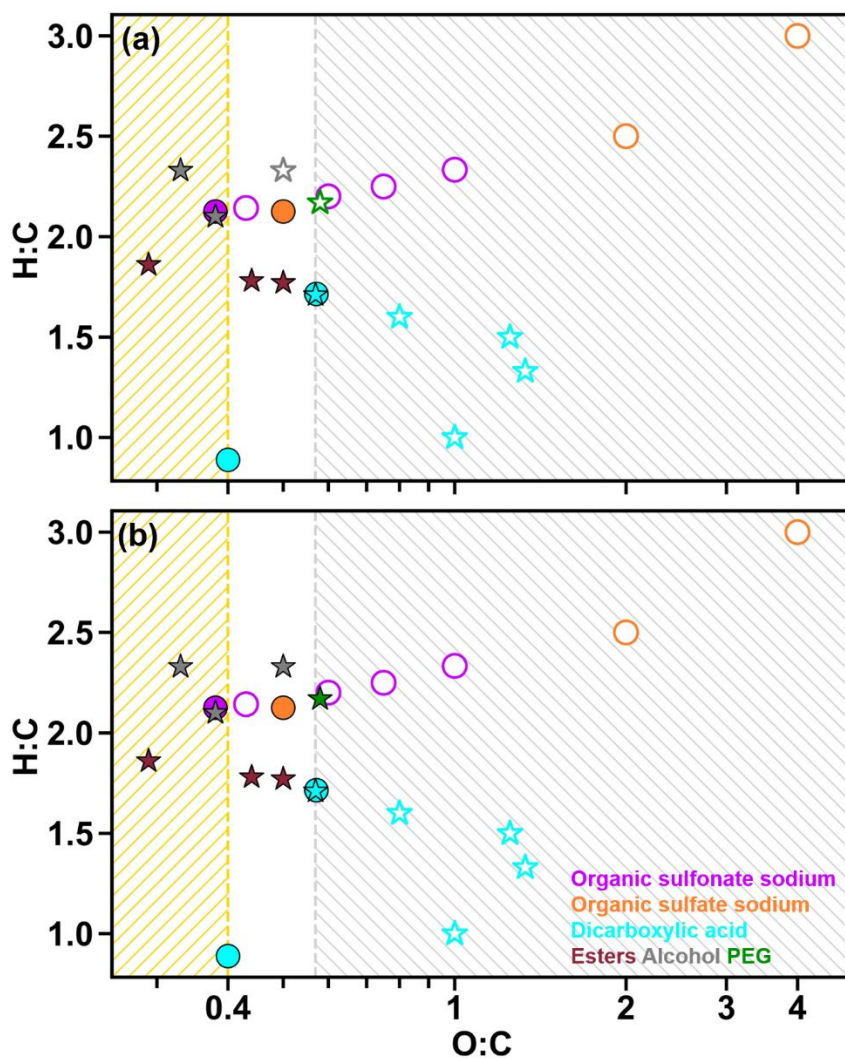
220 The measured SRH values as a function of OVF are plotted in **Fig. 6**. AS-C₈H₁₇SO₄Na showed SRH of 98.7 ± 0.5%
221 when OVF was 70%, higher than those of 50% OVF (82.1 ± 1.6%) and 90% OVF (80.0 ± 0.9%). However, the phenomenon
222 was totally different from that of AS-C₈H₁₇SO₃Na, which showed lower SRH with 70% OVF (62.2 ± 2.6%) than those of 50%
223 OVF (69.6 ± 1.0%) and 90% OVF (81.3 ± 1.2%). Therefore, the above results indicated controversial effect of OVF on SRH
224 (Bertram et al., 2011; Song et al., 2012b).

225



226
227
228
229

Figure 4. ESEM images of (a) homogeneous AS-C₈H₁₇SO₄Na particles (50% OVF) underwent (b) LLPS and (c) efflorescence.



230

231 **Figure 5.** Van Krevelen Diagram for the mixed inorganic–organic particles in the current study (marked as circles): (a) NaCl
232 containing systems and (b) AS containing systems. Solid symbols indicate that LLPS was observed for particles with at least
233 one OVF, while hollow symbols indicate that LLPS was not observed for particles with all tested OVFs. Stars indicate data
234 obtained from You et al. (2013) and O'Brien et al. (2015). PEG represents polyethylene glycol.

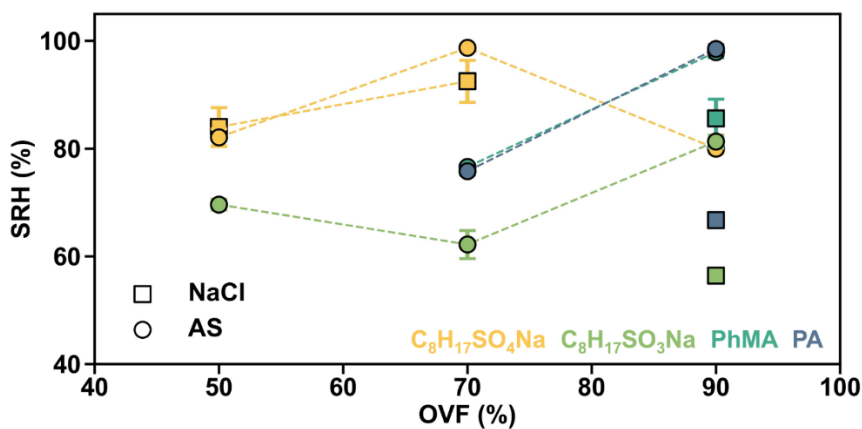


Figure 6. Summary of SRH results as a function of OVF for inorganic-surfactant particles.

235

236

237



238 **Solid phase separation**

239 For mixed systems without undergoing LLPS, we found they were separated with distinct solid phase after obvious
240 efflorescence of inorganic salts (e.g., AS-C₂H₅SO₄Na and NaCl-C₂H₅SO₄Na mixture shown in **Fig. S2**). In **Fig. 7a**, ERH of
241 NaCl-surfactant particles with 50%, 70% and 90% OVF were ranged in 47.0–61.8%, which was higher than the measured
242 ERH (48.3 ± 0.4%) and reported ERH range of pure NaCl (41–51%) (Peng et al., 2022). As for AS-surfactant systems (**Fig.**
243 **7b**), efflorescence was observed for 27 among 30 aerosol samples. We did not observe distinct occurrence of efflorescence for
244 the rest 3 samples, and 2 samples among 3 were with 90% OVF, which could be explained by the possible loss of AS when it
245 was persistently exposed to electronic beam (Posfai et al., 2013; O'brien et al., 2015), especially for particles in which inorganic
246 fractions were small (i.e., high OVF). ERH values of AS-surfactants particles with 50%, 70%, and 90% OVF ranged in
247 31.2–46.6%, showing a close result to the reported ERH of pure AS (30–48%) (Peng et al., 2022), but higher than the measured
248 ERH (30.7 ± 0.9%). The higher efflorescence RH of inorganic-surfactant systems could be explained by the substrate-particle
249 interactions. Ghorai et al. (2014) found an acid displacement reaction in glutaric acid-NaCl systems, which was driven by
250 gaseous HCl liberation and causing chloride depletion. Such interactions of chloride depletion may facilitate efflorescence
251 transitions, resulting in efflorescence at ~ 68% RH and ~ 60% RH, respectively, for internally mixed NaCl-glutaric acid
252 particles with molar ratios of 1:3 and 1:1. Higher ERH could also be attributed to heterogeneous nucleation initiated by
253 chemical purities (Choi and Chan, 2002). Choi and Chan (2002) observed 54.4% ERH for a 1:1 mixed NaCl-glutaric acid, and
254 they explained that insoluble additives crystallized and formed nuclei for the heterogeneous efflorescence of inorganic salts,
255 leading to their higher ERH values.

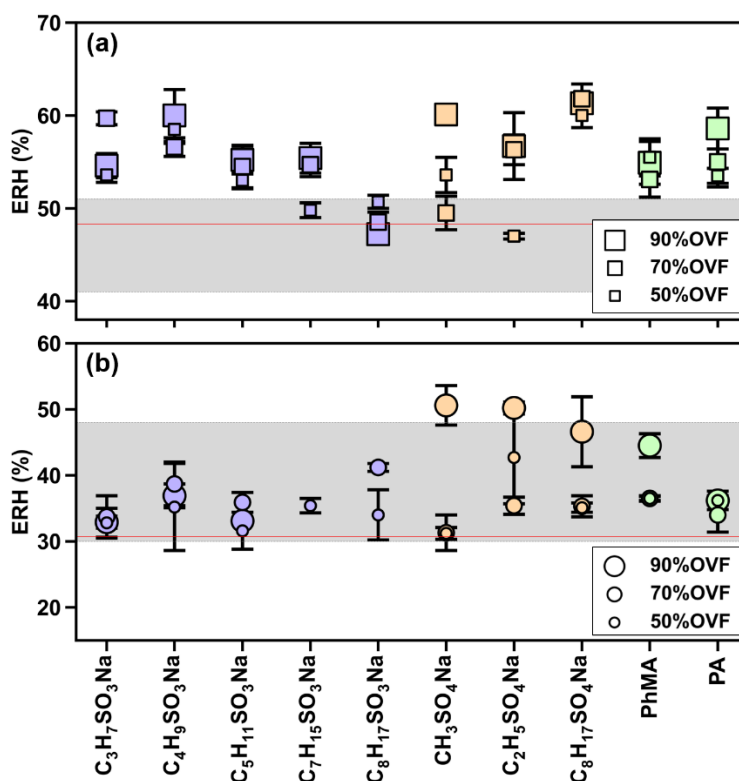
256

257

258



259



260

261

262

263

Figure 7. Measurements of efflorescence relative humidity (ERH) of (a) NaCl-surfactant and (b) AS-surfactant particles. The grey areas in (a) and (b) indicate the efflorescence RH range of NaCl (41–51%) and AS (30–48%) obtained from Peng et al. (2022). Red lines in (a) and (b) represent the measured average ERH of pure NaCl ($48.3 \pm 0.4\%$) and AS ($30.7 \pm 0.9\%$).

264

3.3 Atmospheric implication

265

266

267

268

269

270

Inorganic salts with organic coating are ubiquitous in natural (e.g., marine aerosol) and anthropogenic aerosols (Yu et al., 2019; Li et al., 2021). Based on the direct observation of mixing state for inorganic-surfactants submicron particles, we confirmed an apparent water diffusion hindrance by organic surfactant shell upon hydration, which could notably raise inorganic deliquescence RH to nearly saturated condition. This indicates that the hygroscopicity of aerosol would be reduced in the presence of organic surfactant shell, which might decrease aerosol water content and inhibit aqueous reactions (e.g., aqueous sulfate production).

271

272

273

274

During dehydration, inorganic-surfactant particles were phase-separated before and after efflorescence. Surfactants with lower O:C ratio were more likely to undergo LLPS than those with higher O:C. Compared with homogeneous particles, phase-separated particles could decrease trace gas uptake (You et al., 2012), resulting in reduction of the formation of secondary organic aerosols (SOAs) (Zhang et al., 2018). In addition, organic phase was enriched in “outer shell”, which can



275 potentially alter aerosol water activity and lower aerosol surface tension, hence affecting air-liquid interfacial chemistry as
276 well as aerosol–cloud interactions (Ruehl et al., 2016; Ovadnevaite et al., 2017).

277 We should note that in the atmosphere most particles are smaller (e.g., 0.1 to 0.3 μm) than sample particles and the
278 chemical characteristics of ambient aerosol are not as simple as binary chemical systems in the current study. Therefore, the
279 water kinetic inhibition should be further investigated for smaller particles containing more complex systems in the future. In
280 all, information of mixing states of inorganic–surfactants particles should be incorporated into the atmospheric modeling for
281 heterogeneous chemistry, particle hygroscopicity and growth, to improve predictions on indirect effects of aerosol–climate
282 interactions.

283 4 Conclusions

284 Atmospheric surfactants have potential to distribute to surface, altering mixing state hence influencing aerosol
285 hygroscopicity and CCN activity. But currently direct observation of RH–depended mixing state of aerosol containing
286 atmospheric surfactants is scarce. In this study, dynamic mixing state and phase transitions of 20 types of submicron particles
287 containing inorganic and surface–active organic constituents were directly investigated upon relative humidity (RH) cycling
288 by Environmental Scanning Electron Microscopy (ESEM).

289 Inorganic–organic core-shell morphology was found for dry deposited mixed inorganic–surfactant particles. During
290 hydration, organic shell inhibited water diffusion exposing to inorganic cores, resulting in higher deliquescence RH
291 (88.3–99.5%) of inner inorganic phase compared with pure inorganic aerosol. This was because higher RH may facilitate phase
292 transition of organic shell from solid to semisolid, raising organic viscosity thus decreasing water diffusion exposing to
293 inorganic core. Meanwhile, we directly observed obvious Ostwald ripening of NaCl in single particle, that is, the growth of
294 larger NaCl crystal at the expense of smaller ones, in 6 among 10 NaCl–surfactants systems. As a result of water inhibition by
295 surfactant shell, Ostwald ripening in all systems occurred at RH above 90%, which were higher than reported RH range of
296 pure NaCl measured at 27°C (75–77%).

297 During dehydration, 8 among 20 chemical systems underwent LLPS, including 4 AS–organic systems and 4
298 NaCl–organic systems. LLPS was always observed when $\text{O:C} \leq 0.4$ and never been observed when $\text{O:C} > \sim 0.57$. SRH values
299 of AS–surfactant particles were generally higher than SRH of corresponding NaCl–surfactant systems, which was consistent
300 with reported salting out efficiency of inorganic salts. OVF showed a controversial effect on SRH of inorganic salt–surfactant
301 systems. Additionally, inorganic salts–surfactant systems without LLPS underwent solid phase separation after efflorescence
302 and also showed distinct separated phases. Our results provide a comprehensive and unique insights into the dynamic evolution
303 of inorganic–surfactant particles under fluctuating atmospheric conditions, which could help improve our fundamental
304 knowledge and decrease uncertainty of model estimation on global radiative effect.

305

306 **Data availability.** The data used in this paper can be obtained from the corresponding author upon request.



307

308 **Author contributions.** CX and BK did the experiments, analyzed data. CX plotted the figures and wrote the original draft. FZ
309 and XP contributed to discussion and reviewed the manuscript. BK and ZX reviewed the manuscript and contributed to the
310 fund acquisition. ZW administrated the project, conceptualized the study, reviewed the manuscript and contributed to fund
311 acquisition.

312

313 **Financial support.** The research was supported by National Natural Science Foundation of China (91844301, 41805100,
314 42005087, and 42005086) and the Key Research and Development Program of Zhejiang Province (2021C03165 and
315 2022C03084).

316

317 **Acknowledgment.** We thank Yuzhong Zhang from School of Engineering, Lin Liu and Wenjing Cao from Instrumentation and
318 Service Center for Physical Sciences at Westlake University for the supporting in ESEM experiments.

319

320 **Competing interests.** The authors declare no competing financial interest.

321 Reference

322 Altaf, M. B. and Freedman, M. A.: Effect of Drying Rate on Aerosol Particle Morphology, *J. Phys. Chem. Lett.*, 8,
323 3613-3618, <https://doi.org/10.1021/acs.jpcllett.7b01327>, 2017.

324 Altaf, M. B., Dutcher, D. D., Raymond, T. M., and Freedman, M. A.: Effect of Particle Morphology on Cloud
325 Condensation Nuclei Activity, *ACS Earth Space Chem.*, 2, 634-639,
326 <https://doi.org/10.1021/acsearthspacechem.7b00146>, 2018.

327 Bertram, A. K., Martin, S. T., Hanna, S. J., Smith, M. L., Bodsworth, A., Chen, Q., Kuwata, M., Liu, A., You, Y.,
328 and Zorn, S. R.: Predicting the Relative Humidities of Liquid-Liquid Phase Separation, Efflorescence, and
329 Deliquescence of Mixed Particles of Ammonium Sulfate, Organic Material, and Water Using the Organic-to-
330 Sulfate Mass Ratio of the Particle and the Oxygen-to-Carbon Elemental Ratio of the Organic Component,
331 *Atmos. Chem. Phys.*, 11, 10995-11006, <https://doi.org/10.5194/acp-11-10995-2011>, 2011.

332 Boistelle, R. and Astier, J. P.: Crystallization Mechanisms in Solution, *J. Cryst. Growth*, 90, 14-30,
333 [https://doi.org/10.1016/0022-0248\(88\)90294-1](https://doi.org/10.1016/0022-0248(88)90294-1), 1988.

334 Bruggemann, M., Xu, R. S., Tilgner, A., Kwong, K. C., Mutzel, A., Poon, H. Y., Otto, T., Schaefer, T., Poulain, L.,
335 Chan, M. N., and Herrmann, H.: Organosulfates in Ambient Aerosol: State of Knowledge and Future Research
336 Directions on Formation, Abundance, Fate, and Importance, *Environ. Sci. Technol.*, 54, 3767-3782,



- 337 <https://doi.org/10.1021/acs.est.9b06751>, 2020.
- 338 Cheng, M. Q. and Kuwata, M.: Development of the low-temperature hygroscopicity tandem differential mobility
339 analyzer (Low-T HTDMA) and its application to (NH₄)₂SO₄ and NaCl particles, *J. Aerosol Sci.*, 168, 106111,
340 <https://doi.org/10.1016/j.jaerosci.2022.106111>, 2023.
- 341 Choi, M. Y. and Chan, C. K.: The Effects of Organic Species on the Hygroscopic Behaviors of Inorganic Aerosols,
342 *Environ. Sci. Technol.*, 36, 2422-2428, <https://doi.org/10.1021/es0113293>, 2002.
- 343 Ciobanu, V. G., Marcolli, C., Krieger, U. K., Weers, U., and Peter, T.: Liquid-Liquid Phase Separation in Mixed
344 Organic/Inorganic Aerosol Particles, *J. Phys. Chem. A*, 113, 10966-10978, <https://doi.org/10.1021/jp905054d>,
345 2009.
- 346 Freedman, M. A.: Liquid-Liquid Phase Separation in Supermicrometer and Submicrometer Aerosol Particles, *Acc.*
347 *Chem. Res.*, 53, 1102-1110, <https://doi.org/10.1021/acs.accounts.0c00093>, 2020.
- 348 Ghorai, S., Wang, B. B., Tivanski, A., and Laskin, A.: Hygroscopic Properties of Internally Mixed Particles
349 Composed of NaCl and Water-Soluble Organic Acids, *Environ. Sci. Technol.*, 48, 2234-2241,
350 <https://doi.org/10.1021/es404727u>, 2014.
- 351 Guo, L. Y., Peng, C., Zong, T. M., Gu, W. J., Ma, Q. X., Wu, Z. J., Wang, Z., Ding, X., Hu, M., Wang, X. M., and
352 Tang, M. J.: Comprehensive Characterization of Hygroscopic Properties of Methanesulfonates, *Atmos.*
353 *Environ.*, 224, 117349, <https://doi.org/10.1016/j.atmosenv.2020.117349>, 2020.
- 354 Ho, K. F., Lee, S. C., Ho, S. S. H., Kawamura, K., Tachibana, E., Cheng, Y., and Zhu, T.: Dicarboxylic acids,
355 ketocarboxylic acids, α -dicarbonyls, fatty acids, and benzoic acid in urban aerosols collected during the 2006
356 Campaign of Air Quality Research in Beijing (CAREBeijing-2006), *J. Geophys. Res.: Atmos.*, 115, D19312,
357 <https://doi.org/10.1029/2009jd013304>, 2010.
- 358 Hyder, M., Genberg, J., Sandahl, M., Swietlicki, E., and Jönsson, J. Å.: Yearly trend of dicarboxylic acids in organic
359 aerosols from south of Sweden and source attribution, *Atmos. Environ.*, 57, 197-204,
360 <https://doi.org/10.1016/j.atmosenv.2012.04.027>, 2012.
- 361 Kirpes, R. M., Lei, Z. Y., Fraund, M., Gunsch, M. J., May, N. W., Barrett, T. E., Moffett, C. E., Schauer, A. J.,
362 Alexander, B., Upchurch, L. M., China, S., Quinn, P. K., Moffet, R. C., Laskin, A., Sheesley, R. J., Pratt, K.
363 A., and Ault, A. P.: Solid organic-coated ammonium sulfate particles at high relative humidity in the
364 summertime Arctic atmosphere, *Proc. Natl. Acad. Sci. U.S.A.*, 119, <https://doi.org/ARTN e2104496119>
365 10.1073/pnas.2104496119, 2022.
- 366 Kwamena, N. O. A., Buajareern, J., and Reid, J. P.: Equilibrium Morphology of Mixed Organic/Inorganic/Aqueous



- 367 Aerosol Droplets: Investigating the Effect of Relative Humidity and Surfactants, *J. Phys. Chem. A*, 114, 5787-
368 5795, <https://doi.org/10.1021/jp1003648>, 2010.
- 369 Lambert, F., Kug, J. S., Park, R. J., Mahowald, N., Winckler, G., Abe-Ouchi, A., O'ishi, R., Takemura, T., and Lee,
370 J. H.: The role of mineral-dust aerosols in polar temperature amplification, *Nat. Clim. Change*, 3, 487-491,
371 <https://doi.org/10.1038/Nclimate1785>, 2013.
- 372 Laskin, A., Cowin, J. P., and Iedema, M. J.: Analysis of Individual Environmental Particles using Modern Methods
373 of Electron Microscopy and X-ray Microanalysis, *J. Electron. Spectrosc. Relat. Phenom.*, 150, 260-274,
374 <https://doi.org/10.1016/j.elspec.2005.06.008>, 2006.
- 375 Laskina, O., Morris, H. S., Grandquist, J. R., Qiu, Z., Stone, E. A., Tivanski, A. V., and Grassian, V. H.: Size Matters
376 in the Water Uptake and Hygroscopic Growth of Atmospherically Relevant Multicomponent Aerosol Particles,
377 *J. Phys. Chem. A*, 119, 4489-4497, <https://doi.org/10.1021/jp510268p>, 2015.
- 378 Li, W. J., Shao, L. Y., Zhang, D. Z., Ro, C. U., Hu, M., Bi, X. H., Geng, H., Matsuki, A., Niu, H. Y., and Chen, J.
379 M.: A review of single aerosol particle studies in the atmosphere of East Asia: morphology, mixing state,
380 source, and heterogeneous reactions, *J. Cleaner Prod.*, 112, 1330-1349,
381 <https://doi.org/10.1016/j.jclepro.2015.04.050>, 2016.
- 382 Li, W. J., Teng, X. M., Chen, X. Y., Liu, L., Xu, L., Zhang, J., Wang, Y. Y., Zhang, Y., and Shi, Z. B.: Organic
383 Coating Reduces Hygroscopic Growth of Phase-Separated Aerosol Particles, *Environ. Sci. Technol.*, 55,
384 16339-16346, <https://doi.org/10.1021/acs.est.1c05901>, 2021.
- 385 Martin, S. T.: Phase Transitions of Aqueous Atmospheric Particles, *Chem. Rev.*, 100, 3403-3453,
386 <https://doi.org/10.1021/cr990034t>, 2000.
- 387 Nguyen, Q. T., Kjær, K. H., Kling, K. I., Boesen, T., and Bilde, M.: Impact of Fatty Acid Coating on the CCN
388 Activity of Sea Salt Particles, *Tellus B: Chem. Phys. Meteorol.*, 69, 1304064,
389 <https://doi.org/10.1080/16000889.2017.1304064>, 2017.
- 390 Noziere, B.: Don't Forget the Surface, *Science*, 351, 1396-1397, <https://doi.org/10.1126/science.aaf3253>, 2016.
- 391 O'Brien, R. E., Wang, B. B., Kelly, S. T., Lundt, N., You, Y., Bertram, A. K., Leone, S. R., Laskin, A., and Gilles,
392 M. K.: Liquid-Liquid Phase Separation in Aerosol Particles: Imaging at the Nanometer Scale, *Environ. Sci.*
393 *Technol.*, 49, 4995-5002, <https://doi.org/10.1021/acs.est.5b00062>, 2015.
- 394 Onasch, T. B., Siefert, R. L., Brooks, S. D., Prenni, A. J., Murray, B., Wilson, M. A., and Tolbert, M. A.: Infrared
395 Spectroscopic Study of The Deliquescence and Efflorescence of Ammonium Sulfate Aerosol as a Function of
396 Temperature, *Journal of Geophysical Research-Atmospheres*, 104, 21317-21326,



- 397 <https://doi.org/10.1029/1999jd900384>, 1999.
- 398 Ott, E. J. E. and Freedman, M. A.: Influence of Ions on the Size Dependent Morphology of Aerosol Particles, ACS
399 Earth Space Chem., 5, 2320-2328, <https://doi.org/10.1021/acsearthspacechem.1c00210>, 2021.
- 400 Ovadnevaite, J., Zuend, A., Laaksonen, A., Sanchez, K. J., Roberts, G., Ceburnis, D., Decesari, S., Rinaldi, M.,
401 Hodas, N., Facchini, M. C., Seinfeld, J. H., and O' Dowd, C.: Surface Tension Prevails over Solute Effect in
402 Organic-Influenced Cloud Droplet Activation, Nature, 546, 637-641, <https://doi.org/10.1038/nature22806>,
403 2017.
- 404 Peng, C., Chan, M. N., and Chan, C. K.: The Hygroscopic Properties of Dicarboxylic and Multifunctional Acids:
405 Measurements and UNIFAC Predictions, Environ. Sci. Technol., 35, 4495-4501,
406 <https://doi.org/10.1021/es0107531>, 2001.
- 407 Peng, C., Jing, B., Guo, Y. C., Zhang, Y. H., and Ge, M. F.: Hygroscopic Behavior of Multicomponent Aerosols
408 Involving NaCl and Dicarboxylic Acids, J. Phys. Chem. A, 120, 1029-1038,
409 <https://doi.org/10.1021/acs.jpca.5b09373>, 2016.
- 410 Peng, C., Chen, L., and Tang, M.: A Database for Deliquescence and Efflorescence Relative Humidities of
411 Compounds with Atmospheric Relevance, Fundam. Res., 2, 578-587,
412 <https://doi.org/10.1016/j.fmre.2021.11.021>, 2022.
- 413 Pöhlker, C., Saturno, J., Krüger, M. L., Förster, J. D., Weigand, M., Wiedemann, K. T., Bechtel, M., Artaxo, P., and
414 Andreae, M. O.: Efflorescence upon Humidification? X-ray Microspectroscopic in situ Observation of
415 Changes in Aerosol Microstructure and Phase State upon Hydration, Geophys. Res. Lett., 41, 3681-3689,
416 <https://doi.org/10.1002/2014gl059409>, 2014.
- 417 Pöschl, U.: Atmospheric Aerosols: Composition, Transformation, Climate and Health Effects, Angew. Chem. Int.
418 Ed., 44, 7520-7540, <https://doi.org/10.1002/anie.200501122>, 2005.
- 419 Posfai, M., Axisa, D., Tompa, E., Freney, E., Brientjes, R., and Buseck, P. R.: Interactions of Mineral Dust with
420 Pollution and Clouds: An Individual-Particle TEM Study of Atmospheric Aerosol from Saudi Arabia, Atmos.
421 Res., 122, 347-361, <https://doi.org/10.1016/j.atmosres.2012.12.001>, 2013.
- 422 Reed, N. W., Wing, B. A., Tolbert, M. A., and Browne, E. C.: Trace H₂S Promotes Organic Aerosol Production and
423 Organosulfur Compound Formation in Archean Analog Haze Photochemistry Experiments, Geophys. Res.
424 Lett., 49, <https://doi.org/10.1029/2021GL097032>, 2022.
- 425 Riemer, N., Ault, A. P., West, M., Craig, R. L., and Curtis, J. H.: Aerosol Mixing State: Measurements, Modeling,
426 and Impacts, Rev. Geophys., 57, 187-249, <https://doi.org/10.1029/2018rg000615>, 2019.



- 427 Römpf, A., Winterhalter, R., and Moortgat, G. K.: Oxodicarboxylic acids in atmospheric aerosol particles, *Atmos.*
428 *Environ.*, 40, 6846-6862, <https://doi.org/10.1016/j.atmosenv.2006.05.053>, 2006.
- 429 Roy, P., Mael, L. E., Makhnenko, I., Martz, R., Grassian, V. H., and Dutcher, C. S.: Temperature-Dependent Phase
430 Transitions of Aqueous Aerosol Droplet Systems in Microfluidic Traps, *ACS Earth Space Chem.*, 4, 1527-
431 1539, <https://doi.org/10.1021/acsearthspacechem.0c00114>, 2020.
- 432 Ruehl, C. R. and Wilson, K. R.: Surface Organic Monolayers Control the Hygroscopic Growth of Submicrometer
433 Particles at High Relative Humidity, *J. Phys. Chem. A*, 118, 3952-3966, <https://doi.org/10.1021/jp502844g>,
434 2014.
- 435 Ruehl, C. R., Davies, J. F., and Wilson, K. R.: An Interfacial Mechanism for Cloud Droplet Formation on Organic
436 Aerosols, *Science*, 351, 1447-1450, <https://doi.org/10.1126/science.aad4889>, 2016.
- 437 Shiraiwa, M., Zuend, A., Bertram, A. K., and Seinfeld, J. H.: Gas-Particle Partitioning of Atmospheric Aerosols:
438 Interplay of Physical State, Non-Ideal Mixing and Morphology, *Physical Chemistry Chemical Physics*, 15,
439 11441-11453, <https://doi.org/10.1039/c3cp51595h>, 2013.
- 440 Song, M., Marcolli, C., Krieger, U. K., Zuend, A., and Peter, T.: Liquid-Liquid Phase Separation in Aerosol Particles:
441 Dependence on O:C, Organic Functionalities, and Compositional Complexity, *Geophys. Res. Lett.*, 39,
442 L19801, <https://doi.org/10.1029/2012gl052807>, 2012a.
- 443 Song, M., Marcolli, C., Krieger, U. K., Zuend, A., and Peter, T.: Liquid-Liquid Phase Separation and Morphology
444 of Internally Mixed Dicarboxylic Acids/Ammonium Sulfate/Water Particles, *Atmos. Chem. Phys.*, 12, 2691-
445 2712, <https://doi.org/10.5194/acp-12-2691-2012>, 2012b.
- 446 Song, M., Maclean, A. M., Huang, Y. Z., Smith, N. R., Blair, S. L., Laskin, J., Laskin, A., DeRieux, W. S. W., Li,
447 Y., Shiraiwa, M., Nizkorodov, S. A., and Bertram, A. K.: Liquid-Liquid Phase Separation and Viscosity within
448 Secondary Organic Aerosol Generated from Diesel Fuel Vapors, *Atmos. Chem. Phys.*, 19, 12515-12529,
449 <https://doi.org/10.5194/acp-19-12515-2019>, 2019.
- 450 Song, M. J., Liu, P. F., Martin, S. T., and Bertram, A. K.: Liquid-Liquid Phase Separation in Particles Containing
451 Secondary Organic Material Free of Inorganic Salts, *Atmos. Chem. Phys.*, 17, 11261-11271,
452 <https://doi.org/10.5194/acp-17-11261-2017>, 2017.
- 453 Takahama, S., Pathak, R. K., and Pandis, S. N.: Efflorescence Transitions of Ammonium Sulfate Particles Coated
454 with Secondary Organic Aerosol, *Environ. Sci. Technol.*, 41, 2289-2295, <https://doi.org/10.1021/es0619915>,
455 2007.
- 456 Ting, Y. C., Mitchell, E. J. S., Allan, J. D., Liu, D. T., Spracklen, D. V., Williams, A., Jones, J. M., Lea-Langton, A.



- 457 R., McFiggans, G., and Coe, H.: Mixing State of Carbonaceous Aerosols of Primary Emissions from
458 "Improved" African Cookstoves, *Environ. Sci. Technol.*, 52, 10134-10143,
459 <https://doi.org/10.1021/acs.est.8b00456>, 2018.
- 460 Tolocka, M. P. and Turpin, B.: Contribution of Organosulfur Compounds to Organic Aerosol Mass, *Environ. Sci.*
461 *Technol.*, 46, 7978-7983, <https://doi.org/10.1021/es300651v>, 2012.
- 462 Unga, F., Choel, M., Derimian, Y., Deboudt, K., Dubovik, O., and Goloub, P.: Microscopic Observations of Core-
463 Shell Particle Structure and Implications for Atmospheric Aerosol Remote Sensing, *Journal of Geophysical*
464 *Research-Atmospheres*, 123, 13944-13962, <https://doi.org/10.1029/2018jd028602>, 2018.
- 465 Voorhees, P. W.: The Theory of Ostwald Ripening, *J. Stat. Phys.*, 38, 231-252, <https://doi.org/10.1007/Bf01017860>,
466 1985.
- 467 Wang, W. H., Shao, L. Y., Mazzoleni, C., Li, Y. W., Kotthaus, S., Grimmond, S., Bhandari, J., Xing, J. P., Feng, X.
468 L., Zhang, M. Y., and Shi, Z. B.: Measurement report: Comparison of wintertime individual particles at ground
469 level and above the mixed layer in urban Beijing, *Atmos. Chem. Phys.*, 21, 5301-5314,
470 <https://doi.org/10.5194/acp-21-5301-2021>, 2021.
- 471 Wise, M. E., Martin, S. T., Russell, L. M., and Buseck, P. R.: Water Uptake by NaCl Particles Prior to Deliquescence
472 and the Phase Rule, *Aerosol Sci. Technol.*, 42, 281-294, <https://doi.org/10.1080/02786820802047115>, 2008.
- 473 Xiong, C., Chen, X. Y., Ding, X. L., Kuang, B. Y., Pei, X. Y., Xu, Z. N., Yang, S. K., Hu, H., and Wang, Z. B.:
474 Reconsideration of Surface Tension and Phase State Effects on Cloud Condensation Nuclei Activity Based on
475 the Atomic Force Microscopy Measurement, *Atmos. Chem. Phys.*, 22, 16123-16135,
476 <https://doi.org/10.5194/acp-22-16123-2022>, 2022.
- 477 Xu, L., Fukushima, S., Sobanska, S., Murata, K., Naganuma, A., Liu, L., Wang, Y. Y., Niu, H. Y., Shi, Z. B., Kojima,
478 T., Zhang, D. Z., and Li, W. J.: Tracing the evolution of morphology and mixing state of soot particles along
479 with the movement of an Asian dust storm, *Atmos. Chem. Phys.*, 20, 14321-14332,
480 <https://doi.org/10.5194/acp-20-14321-2020>, 2020.
- 481 Xu, W. Q., Chen, C., Qiu, Y. M., Li, Y., Zhang, Z. Q., Karnezi, E., Pandis, S. N., Xie, C. H., Li, Z. J., Sun, J. X.,
482 Ma, N., Xu, W. Y., Fu, P. Q., Wang, Z. F., Zhu, J., Worsnop, D. R., Ng, N. L., and Sun, Y. L.: Organic aerosol
483 volatility and viscosity in the North China Plain: contrast between summer and winter, *Atmos. Chem. Phys.*,
484 21, 5463-5476, <https://doi.org/10.5194/acp-21-5463-2021>, 2021.
- 485 You, Y., Renbaum-Wolff, L., Carreras-Sospedra, M., Hanna, S. J., Hiranuma, N., Kamal, S., Smith, M. L., Zhang,
486 X. L., Weber, R. J., Shilling, J. E., Dabdub, D., Martin, S. T., and Bertram, A. K.: Images Reveal that



- 487 Atmospheric Particles can Undergo Liquid-Liquid Phase Separations, *Proc. Natl. Acad. Sci. U.S.A.*, 109,
488 13188-13193, <https://doi.org/10.1073/pnas.1206414109>, 2012.
- 489 You, Y., Renbaum-Wolff, L., and Bertram, A. K.: Liquid-Liquid Phase Separation in Particles Containing Organics
490 Mixed with Ammonium Sulfate, Ammonium Bisulfate, Ammonium Nitrate or Sodium Chloride, *Atmos.*
491 *Chem. Phys.*, 13, 11723-11734, <https://doi.org/10.5194/acp-13-11723-2013>, 2013.
- 492 You, Y. and Bertram, A. K.: Effects of Molecular Weight and Temperature on Liquid-Liquid Phase Separation in
493 Particles Containing Organic Species and Inorganic Salts, *Atmos. Chem. Phys.*, 15, 1351-1365,
494 <https://doi.org/10.5194/acp-15-1351-2015>, 2015.
- 495 Yu, H., Li, W. J., Zhang, Y. M., Tunved, P., Dall'Osto, M., Shen, X. J., Sun, J. Y., Zhang, X. Y., Zhang, J. C., and
496 Shi, Z. B.: Organic Coating on Sulfate and Soot Particles during Late Summer in the Svalbard Archipelago,
497 *Atmos. Chem. Phys.*, 19, 10433-10446, <https://doi.org/10.5194/acp-19-10433-2019>, 2019.
- 498 Zavacka, K., Nedela, V., Olbert, M., Tihlarikova, E., Vetrakova, L., Yang, X., and Heger, D.: Temperature and
499 Concentration Affect Particle Size Upon Sublimation of Saline Ice: Implications for Sea Salt Aerosol
500 Production in Polar Regions, *Geophys. Res. Lett.*, 49, <https://doi.org/ARTN e2021GL097098>
501 10.1029/2021GL097098, 2022.
- 502 Zeng, G., Kelley, J., Kish, J. D., and Liu, Y.: Temperature-Dependent Deliquescent and Efflorescent Properties of
503 Methanesulfonate Sodium Studied by ATR-FTIR Spectroscopy, *J. Phys. Chem. A*, 118, 583-591,
504 <https://doi.org/10.1021/jp405896y>, 2014.
- 505 Zhang, J., Yuan, Q., Liu, L., Wang, Y. Y., Zhang, Y. X., Xu, L., Pang, Y., Zhu, Y. H., Niu, H. Y., Shao, L. Y., Yang,
506 S. S., Liu, H., Pan, X. L., Shi, Z. B., Hu, M., Fu, P. Q., and Li, W. J.: Trans-Regional Transport of Haze
507 Particles From the North China Plain to Yangtze River Delta During Winter, *Journal of Geophysical Research-*
508 *Atmospheres*, 126, <https://doi.org/ARTN e2020JD033778>
509 10.1029/2020JD033778, 2021.
- 510 Zhang, J., Wang, Y. Y., Teng, X. M., Liu, L., Xu, Y. S., Ren, L. H., Shi, Z. B., Zhang, Y., Jiang, J. K., Liu, D. T., Hu,
511 M., Shao, L. Y., Chen, J. M., Martin, S. T., Zhang, X. Y., and Li, W. J.: Liquid-Liquid Phase Separation Reduces
512 Radiative Absorption by Aged Black Carbon Aerosols, *Commun. Earth Environ.*, 3, 128,
513 <https://doi.org/10.1038/s43247-022-00462-1>, 2022.
- 514 Zhang, Y., Chen, Y. Z., Lambe, A. T., Olson, N. E., Lei, Z. Y., Craig, R. L., Zhang, Z. F., Gold, A., Onasch, T. B.,
515 Jayne, J. T., Worsnop, D. R., Gaston, C. J., Thornton, J. A., Vizuete, W., Ault, A. P., and Surratt, J. D.: Effect
516 of the Aerosol-Phase State on Secondary Organic Aerosol Formation from the Reactive Uptake of Isoprene-



517 Derived Epoxydiols (IEPDX), Environ. Sci. Technol. Lett., 5, 167-174,
518 <https://doi.org/10.1021/acs.estlett.8b00044>, 2018.

519 Zhang, Y. X., Zhang, Q., Yao, Z. L., and Li, H. Y.: Particle Size and Mixing State of Freshly Emitted Black Carbon
520 from Different Combustion Sources in China, Environ. Sci. Technol., 54, 7766-7774,
521 <https://doi.org/10.1021/acs.est.9b07373>, 2020.

522 Zhu, Y., Pang, S., and Zhang, Y.: Observations on the unique phase transitions of inorganics relevant due to gluconic
523 acid in particles, Atmos. Environ., 288, 119313, <https://doi.org/10.1016/j.atmosenv.2022.119313>, 2022.

524